

Light neutralinos at LHC in cosmologically–inspired scenarios: new benchmarks in the search for supersymmetry

A. Bottino,¹ N. Fornengo,¹ G. Polesello,² and S. Scopel³

¹*Dipartimento di Fisica Teorica, Università di Torino
Istituto Nazionale di Fisica Nucleare, Sezione di Torino
via P. Giuria 1, I-10125 Torino, Italy*

²*Istituto Nazionale di Fisica Nucleare, Sezione di Pavia
via Bassi 6, 27100 Pavia Italy*

³*Korea Institute for Advanced Study
Seoul 130-722, Korea*

(Dated: November 3, 2018)

We study how the properties of the four neutralino states, χ_i ($i = 1, 2, 3, 4$), can be investigated at the Large Hadron Collider (LHC), in the case when the lightest one, χ_1 , has a mass $m_\chi \lesssim 50$ GeV and is stable. This situation arises naturally in supersymmetric models where gaugino masses are not unified at a Grand Unified (GUT) scale and R-parity is conserved. The main features of these neutralino states are established by analytical and numerical analyses, and two scenarios are singled out on the basis of the cosmological properties required for the relic neutralinos. Signals expected at LHC are discussed through the main chain processes started by a squark, produced in the initial proton-proton scattering. We motivate the selection of some convenient benchmarks, in the light of the spectroscopical properties (mass spectrum and transitions) of the four neutralino states. Branching ratios and the expected total number of events are derived in the various benchmarks, and their relevance for experimental determination of neutralino properties is finally discussed.

PACS numbers: 95.35.+d,11.30.Pb,12.60.Jv,95.30.Cq

I. INTRODUCTION

Light neutralinos, *i.e.* neutralinos with a mass $m_\chi \lesssim 50$ GeV, arise naturally in supersymmetric models where gaugino masses are not unified at a Grand Unified (GUT) scale. When R-parity conservation is assumed, these neutralinos offer a very rich phenomenology under various cosmological and astrophysical aspects [1, 2].

In the present paper we study how these light neutralinos can be investigated at the Large Hadron Collider (LHC), which will soon start being operated at CERN [3, 4].

To this purpose we first delineate what are the main properties of the four neutralino states, χ_i ($i = 1, 2, 3, 4$), in the case when the lightest one, χ_1 (or χ in short), has a mass $m_\chi \lesssim 50$ GeV. This neutralino is stable, in case it occurs to be the Lightest Supersymmetric Particle and R-parity is conserved. In particular, special asymptotic schemes for the four neutralino states are analysed: two hierarchical schemes (with so-called normal and inverted hierarchy, respectively) and an almost degenerate one.

Once the properties of all the neutralino states are established by analytical and numerical analyses, two main scenarios are singled out on the basis of the cosmological properties required for the relic neutralinos.

Then, we analyse the signals expected at LHC, in terms of the main chain processes which are initiated by a squark and lead finally to χ_1 through an intermediate production of χ_i ($i = 2, 3, 4$). We evaluate the branching ratios for the various processes and discuss their features in terms of the spectroscopic properties (mass spectrum and transitions) of the four neutralino states. Various benchmarks of special physical interest are considered.

The total number of events expected for these processes at LHC is estimated for a typical representative value of the integrated luminosity and their relevance for experimental determination of neutralino properties is finally discussed.

The scheme of our paper is the following. The features of the employed supersymmetric model are presented in Sect. II, where also the main structural properties of the four neutralino states are described. In Sect. III we delineate

the scenarios imposed by cosmology on light relic neutralinos. In Sect. IV we derive branching ratios and the total number of events expected at LHC. Finally, conclusions are drawn in Sect. V.

II. THE SUPERSYMMETRIC MODEL

The supersymmetric scheme we employ in the present paper is the one described in Ref. [1]: an effective MSSM scheme (effMSSM) at the electroweak scale, with the following independent parameters: $M_1, M_2, M_3, \mu, \tan \beta, m_A, m_{\tilde{q}}, m_{\tilde{l}}$ and A . Notations are as follows: M_1, M_2 and M_3 are the U(1), SU(2) and SU(3) gaugino masses (these parameters are taken here to be positive), μ is the Higgs mixing mass parameter, $\tan \beta$ the ratio of the two Higgs v.e.v.'s, m_A the mass of the CP-odd neutral Higgs boson, $m_{\tilde{q}}$ is a squark soft-mass common to all squarks, $m_{\tilde{l}}$ is a slepton soft-mass common to all sleptons, and A is a common dimensionless trilinear parameter for the third family, $A_{\tilde{b}} = A_{\tilde{t}} \equiv Am_{\tilde{q}}$ and $A_{\tilde{\tau}} \equiv Am_{\tilde{l}}$ (the trilinear parameters for the other families being set equal to zero). In our model, no gaugino mass unification at a Grand Unified (GUT) scale is assumed. The following experimental constraints are imposed: accelerators data on supersymmetric and Higgs boson searches (CERN e^+e^- collider LEP2 [5] and Collider Detectors D0 and CDF at Fermilab [6]); measurements of the $b \rightarrow s + \gamma$ decay process [7]: $2.89 \leq B(b \rightarrow s + \gamma) \cdot 10^4 \leq 4.21$ is employed here (this interval is larger by 25% with respect to the experimental determination [7] in order to take into account theoretical uncertainties in the supersymmetric (SUSY) contributions [8] to the branching ratio of the process (for the Standard Model calculation, we employ the recent NNLO results from Ref. [9])); the upper bound on the branching ratio $BR(B_s^0 \rightarrow \mu^- + \mu^+)$ [10]: we take $BR(B_s^0 \rightarrow \mu^- + \mu^+) < 1.2 \cdot 10^{-7}$; measurements of the muon anomalous magnetic moment $a_\mu \equiv (g_\mu - 2)/2$: for the deviation Δa_μ of the experimental world average from the theoretical evaluation within the Standard Model we use here the range $-98 \leq \Delta a_\mu \cdot 10^{11} \leq 565$, derived from the latest experimental [11] and theoretical [12] data.

A. Composition of the neutralino states

The linear superpositions of bino \tilde{B} , wino $\tilde{W}^{(3)}$ and of the two Higgsino states $\tilde{H}_1^\circ, \tilde{H}_2^\circ$ which define the four neutralino states are written in the following way:

$$\chi_i \equiv a_1^{(i)} \tilde{B} + a_2^{(i)} \tilde{W}^{(3)} + a_3^{(i)} \tilde{H}_1^\circ + a_4^{(i)} \tilde{H}_2^\circ \quad (i = 1, 2, 3, 4). \quad (1)$$

These states diagonalize the mass matrix

$$\begin{pmatrix} M_1 & 0 & -m_Z s_\theta c_\beta & m_Z s_\theta s_\beta \\ 0 & M_2 & m_Z c_\theta c_\beta & -m_Z c_\theta s_\beta \\ -m_Z s_\theta c_\beta & m_Z c_\theta c_\beta & 0 & -\mu \\ m_Z s_\theta s_\beta & -m_Z c_\theta s_\beta & -\mu & 0 \end{pmatrix}, \quad (2)$$

where $s_\beta \equiv \sin \beta$, $c_\beta \equiv \cos \beta$, and $s_\theta \equiv \sin \theta$, $c_\theta \equiv \cos \theta$, θ being the Weinberg angle. The mass eigenvalues (with signs) will be denoted by m_i . The smallest mass eigenvalue $|m_1|$ will also be denoted by m_χ .

From the set of equations

$$\begin{aligned} (M_1 - m_i) a_1^{(i)} - m_Z s_\theta c_\beta a_3^{(i)} + m_Z s_\theta s_\beta a_4^{(i)} &= 0 \\ (M_2 - m_i) a_2^{(i)} + m_Z c_\theta c_\beta a_3^{(i)} - m_Z c_\theta s_\beta a_4^{(i)} &= 0 \\ -m_Z s_\theta c_\beta a_1^{(i)} + m_Z c_\theta c_\beta a_2^{(i)} - m_i a_3^{(i)} - \mu a_4^{(i)} &= 0 \\ m_Z s_\theta s_\beta a_1^{(i)} - m_Z c_\theta s_\beta a_2^{(i)} - \mu a_3^{(i)} - m_i a_4^{(i)} &= 0, \end{aligned} \quad (3)$$

that follow from the diagonalization of the mass matrix of Eq. (2), one obtains the ratios

$$\frac{a_2^{(i)}}{a_1^{(i)}} = -\frac{M_1 - m_i}{M_2 - m_i} \cot \theta$$

$$\begin{aligned}\frac{a_3^{(i)}}{a_1^{(i)}} &= \frac{m_Z(m_i c_\beta + \mu s_\beta)(s_\theta^2 M_2 + c_\theta^2 M_1 - m_i)}{s_\theta(M_2 - m_i)(\mu^2 - m_i^2)} \\ \frac{a_3^{(i)}}{a_4^{(i)}} &= -\frac{m_i c_\beta + \mu s_\beta}{\mu c_\beta + m_i s_\beta},\end{aligned}\quad (4)$$

which, together with the normalization conditions, provide the compositions of the four neutralino states [13].

The LEP lower limit on the chargino mass ($m_{\chi^\pm} \gtrsim 100$ GeV) sets a lower bound on both $|\mu|$ and M_2 : $|\mu|, M_2 \gtrsim 100$ GeV. Since, on the contrary, M_1 is unbound, the lowest value for m_χ occurs when

$$m_\chi \simeq M_1 \ll |\mu|, M_2. \quad (5)$$

Thus, $\chi \equiv \chi_1$ is mainly a Bino, whose mixings with the other interaction eigenstates are readily derived from Eqs. (4) to be

$$\frac{a_2^{(1)}}{a_1^{(1)}} \simeq \frac{\xi_1}{M_2} \cot\theta, \quad \frac{a_3^{(1)}}{a_1^{(1)}} \simeq s_\theta s_\beta \frac{m_Z}{\mu}, \quad \frac{a_3^{(1)}}{a_4^{(1)}} \simeq -\frac{\mu s_\beta}{M_1 s_\beta + \mu c_\beta}, \quad (6)$$

where $\xi_1 \equiv m_1 - M_1$. Notice that, in deriving Eq. (5), we have also taken into account that in the present paper we will only consider $\tan\beta \geq 10$.

From Eqs. (4) one also obtains approximate expressions for the compositions of the eigenstates which correspond to the asymptotic mass eigenvalues: $m_i \sim \pm\mu$ and $m_i \sim M_2$. That is:

a) for the neutralino states χ_i with $m_i \simeq \pm\mu$,

$$\frac{a_2^{(i)}}{a_1^{(i)}} \simeq \frac{\pm\mu}{M_2 \mp \mu} \cot\theta, \quad \frac{a_3^{(i)}}{a_3^{(i)}} \simeq \frac{2\xi_2 s_\theta (\pm\mu - M_2)}{M_Z s_\beta (s_\theta^2 M_2 \mp \mu)}, \quad \frac{a_3^{(i)}}{a_4^{(i)}} \simeq \mp 1 + \frac{\xi_2}{\mu}, \quad (7)$$

where $\xi_2 \equiv \pm\mu - m_i$.

b) for the neutralino state χ_i with $m_i \simeq M_2$,

$$\frac{a_1^{(i)}}{a_2^{(i)}} \simeq \frac{\xi_3}{M_2} \tan\theta, \quad \frac{a_1^{(i)}}{a_3^{(i)}} \simeq \frac{\xi_3 s_\theta (M_2^2 - \mu^2)}{M_Z (M_2 c_\beta + \mu s_\beta) c_\theta^2 M_2}, \quad \frac{a_3^{(i)}}{a_4^{(i)}} \simeq -\frac{\mu s_\beta + M_2 c_\beta}{M_2 s_\beta + \mu c_\beta}, \quad (8)$$

where $\xi_3 \equiv M_2 - m_i$.

For illustrative purposes, in Figs.1–2 we show the results of the numerical diagonalization of the matrix of Eq. (2) versus M_2 , for the representative point defined by the following values of the other supersymmetric parameters which enter in the mass matrix of Eq. (2): $M_1 = 25$ GeV, $\mu = 300$ GeV, $\tan\beta = 10$. Fig. 1 displays the behaviour of the mass eigenvalues $|m_i|$, Fig. 2 the compositions of the states χ_i .

The approximate analytic expressions in Eqs. (6-8) and the numerical results in Fig. 2 display quantitatively the following properties: (i) χ_1 is mainly a B-ino whose mixing with \tilde{H}_1° is sizable at small μ , (ii) χ_3 has a mass $|m_3| \simeq |\mu|$ with a large $\tilde{H}_1^\circ - \tilde{H}_2^\circ$ mixing, independently of M_2 , (iii) χ_2 and χ_4 interchange their main structures depending on the value of the ratio $|\mu|/M_2$: χ_2 is dominantly a W-ino (with a sizable subdominance of \tilde{H}_1°) for $M_2 \ll |\mu|$ and a maximal $\tilde{H}_1^\circ - \tilde{H}_2^\circ$ admixture for $M_2 \gg |\mu|$, whereas χ_4 is a maximal $\tilde{H}_1^\circ - \tilde{H}_2^\circ$ admixture for $M_2 \ll |\mu|$ and a very pure W-ino for $M_2 \gg |\mu|$. Also their properties relevant to the case $M_2 \sim |\mu|$ are transparent from Eqs. (6-8) and Fig. 2.

Depending on the relative values of the parameters M_2 and μ , it is useful, for the discussion to be developed later, to define the following neutralino spectroscopic schemes (notice that we always assume $(M_1 \ll M_2, |\mu|)$): (i) normal hierarchical scheme ($M_2 < |\mu|$), (ii) degenerate scheme ($M_2 \sim |\mu|$), (iii) inverted hierarchical scheme ($M_2 > |\mu|$). These schemes are depicted in Fig. 3.

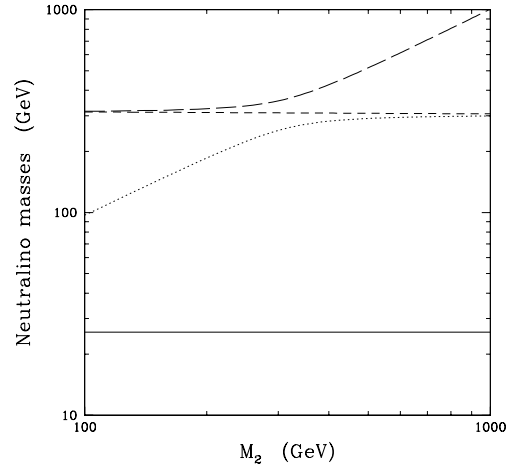


FIG. 1: Neutralino masses as functions of M_2 for $M_1 = 25$ GeV, $\mu = 300$ GeV and $\tan\beta = 10$.

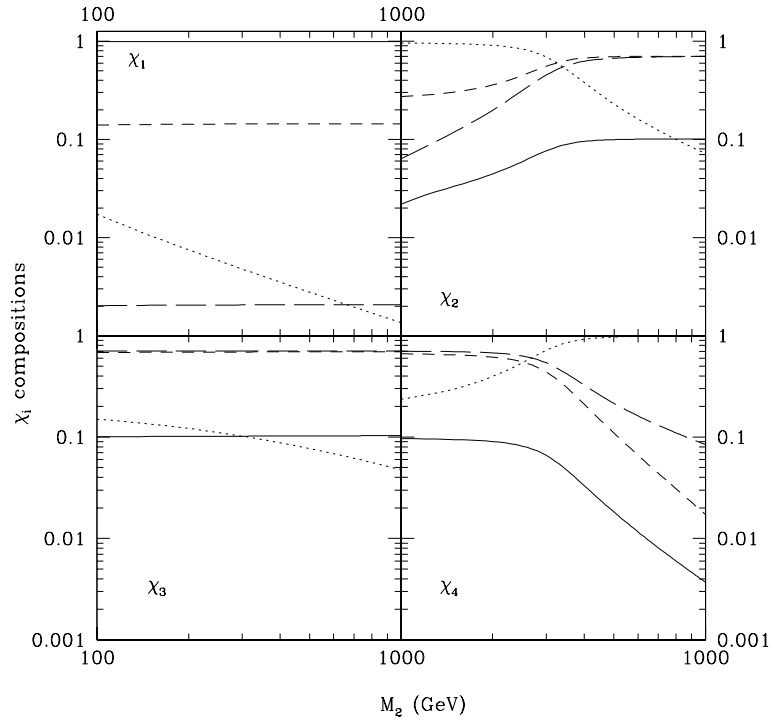


FIG. 2: Compositions of the neutralino states χ_i as functions of M_2 for $M_1 = 25$ GeV, $\mu = 300$ GeV and $\tan\beta = 10$. Up-left panel: χ_1 , up-right panel: χ_2 , bottom-left panel: χ_3 , bottom-right panel: χ_4 . Solid lines denote $|a_1^i|$, dotted lines $|a_2^i|$, short-dashed lines $|a_3^i|$, long-dashed lines $|a_4^i|$.

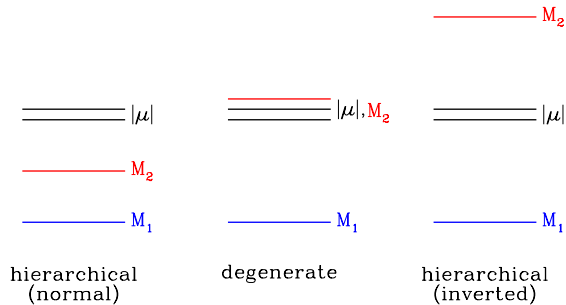


FIG. 3: Asymptotic spectroscopic schemes for the χ_i ($i = 1, 2, 3, 4$) neutralino states .

B. Cosmological properties

As discussed in Ref. [1], under the assumption that R-parity is conserved, the lower bound on the neutralino mass m_χ is provided by the upper bound on the relic abundance for cold dark matter (CDM), $\Omega_{CDM}h^2$.

We recall that the neutralino relic abundance is given by

$$\Omega_\chi h^2 = \frac{x_f}{g_\star(x_f)^{1/2}} \frac{3.3 \cdot 10^{-38} \text{ cm}^2}{\langle \widetilde{\sigma}_{ann} v \rangle}, \quad (9)$$

where $\langle \widetilde{\sigma}_{ann} v \rangle \equiv x_f \langle \sigma_{ann} v \rangle_{\text{int}}$, $\langle \sigma_{ann} v \rangle_{\text{int}}$ being the integral from the present temperature up to the freeze-out temperature T_f of the thermally averaged product of the annihilation cross-section times the relative velocity of a pair of neutralinos, x_f is defined as $x_f \equiv \frac{m_\chi}{T_f}$ and $g_\star(x_f)$ denotes the relativistic degrees of freedom of the thermodynamic bath at x_f . For $\langle \widetilde{\sigma}_{ann} v \rangle$ we use here the standard expansion in S and P waves: $\langle \widetilde{\sigma}_{ann} v \rangle \simeq \tilde{a} + \tilde{b}(2x_f)^{-1}$.

A host of cosmological observations imply that the cold dark matter content has to stay in the range $0.092 \leq \Omega_{CDM}h^2 \leq 0.124$ [14]. Thus the supersymmetric configurations have to satisfy the cosmological constraint $\Omega_\chi h^2 \leq (\Omega_{CDM}h^2)_{max} = 0.124$.

III. SCENARIOS FOR LIGHT NEUTRALINOS

In Ref. [1] it is shown that the cosmological condition $\Omega_\chi h^2 \leq (\Omega_{CDM}h^2)_{max} = 0.124$ provides a lower limit $m_\chi \gtrsim 7$ GeV. Such a situation occurs when $M_1 \sim 10$ GeV and $\langle \widetilde{\sigma}_{ann} v \rangle \simeq \tilde{a}$ receives a sizable contribution by the exchange of the A Higgs boson in the s channel. This, in turn, happens when the two following conditions are met: a) m_A is as small as its experimental lower bound, $m_A = 90$ GeV, b) the B-ino component of the χ_1 configuration is maximally mixed with the \tilde{H}_1° component (*i. e.* $\frac{a_3^{(1)}}{a_1^{(1)}} \simeq 0.4$). From the second expression in Eq. (6) one sees that condition (b) is satisfied when μ is small ($|\mu| \sim 100$ -200 GeV). Moreover, it turns out that $\tan\beta$ must be large ($\tan\beta \sim 30 - 45$) in order for the annihilation cross section through the exchange of the A Higgs boson to be sizable. Finally, the trilinear coupling is mildly constrained to stay in the interval $-1 \lesssim A \lesssim +1$.

In the following we will characterize such a set of supersymmetric parameters as **Scenario A**. More specifically, this scenario is identified by the following sector of the supersymmetric parameter space: $M_1 \sim 10$ GeV, $|\mu| \sim (100 - 200)$ GeV, $m_A \sim 90$ GeV, $\tan\beta \sim 30 - 45$, $-1 \lesssim A \lesssim +1$; the other supersymmetric parameters are not *a priori* fixed.

From Eqs. (6) it turns out that, in this scenario, the following hierarchy holds for the coefficients $a_i^{(1)}$ of χ_1

$$|a_1^{(1)}| > |a_3^{(1)}| \gg |a_2^{(1)}|, |a_4^{(1)}|. \quad (10)$$

It is proved in Ref. [1] that at small m_χ , when $m_A \gtrsim (200 - 300)$ GeV, the cosmological constraint $\Omega_\chi h^2 \leq (\Omega_{CDM}h^2)_{max}$ is satisfied because of stau-exchange contributions (in the t, u channels) to $\langle \widetilde{\sigma}_{ann} v \rangle$, provided that:

scenario	M_1 [GeV]	$ \mu $ [GeV]	$\tan\beta$	m_A [GeV]	$m_{\tilde{l}}$ [GeV]
\mathcal{A}	~ 10	100–200	30–45	~ 90	–
\mathcal{B}	~ 25	$\gtrsim 500$	$\lesssim 20$	$\gtrsim 200$	100–200

TABLE I: Scenarios for light neutralinos as described in Section III. In scenario \mathcal{A} the slepton soft mass $m_{\tilde{l}}$ is unconstrained: in our analysis a few representative values for $m_{\tilde{l}}$ are considered within its natural range $115 \text{ GeV} \leq m_{\tilde{l}} \leq 1 \text{ TeV}$. Moreover, in scenario \mathcal{A} : $-1 \lesssim A \lesssim +1$, in scenario \mathcal{B} : $-2 \lesssim A \lesssim +2$.

(i) $m_{\tilde{\tau}}$ is sufficiently light, $m_{\tilde{\tau}} \sim 90 \text{ GeV}$ (notice that the current experimental limit is $m_{\tilde{\tau}} \sim 87 \text{ GeV}$) and (ii) χ_1 is a very pure B-ino (*i.e.* $(1 - a_1^{(1)}) = \mathcal{O}(10^{-3})$). In such a situation, the lower limit on the neutralino mass is $m_{\chi} \gtrsim (15 - 18) \text{ GeV}$ [15].

Let us first discuss the implications of the prerequisite (i). The experimental lower bounds on the sneutrino mass and on the charged slepton masses of the first two families imply a lower bound on the soft slepton mass: $m_{\tilde{l}} \gtrsim 115 \text{ GeV}$. In order to make the request $m_{\tilde{\tau}} \sim 90 \text{ GeV}$ compatible with $m_{\tilde{l}} \gtrsim 115 \text{ GeV}$, it is necessary that the off-diagonal terms of the sleptonic mass matrix in the eigenstate basis, which are proportional to $\mu \tan\beta$, are large. Numerically, one finds $|\mu| \tan\beta \sim 5000 \text{ GeV}$.

On the other side, the condition (ii) requires that $a_3^{(1)}/a^{(1)} \lesssim 10^{-1}$, *i. e.*, according to the second expression of Eq. (6), $\frac{a_3^{(1)}}{a_1^{(1)}} \simeq s_{\theta} s_{\beta} \frac{m_Z}{\mu} \lesssim 10^{-1}$. Combining this last expression with the condition $|\mu| \tan\beta \sim 5000 \text{ GeV}$, one finds that $|\mu|$ and $\tan\beta$ are bounded by: $|\mu| \gtrsim 500 \text{ GeV}$, $\tan\beta \lesssim 10$. These bounds are somewhat weaker for values of the neutralino mass larger than $\sim 15\text{--}18 \text{ GeV}$.

The previous arguments lead us to introduce a new scenario, denoted as **Scenario \mathcal{B}** , identified by the following sector of the supersymmetric parameter space: $M_1 \sim 25 \text{ GeV}$, $|\mu| \gtrsim 500 \text{ GeV}$, $\tan\beta \lesssim 20$; $m_{\tilde{l}} \gtrsim (100 - 200) \text{ GeV}$, $-2.5 \lesssim A \lesssim +2.5$; the other supersymmetric parameters are not *a priori* fixed.

From Eqs. (6) it turns out that, in this scenario, the following hierarchy holds for the coefficients $a_i^{(1)}$ of χ_1

$$|a_1^{(1)}| \gg |a_3^{(1)}|, |a_2^{(1)}|, |a_4^{(1)}|. \quad (11)$$

The features of scenarios \mathcal{A} and \mathcal{B} are summarized in Table I.

IV. SIGNALS AT LHC

If kinematically accessible, squarks and gluinos are expected to be copiously produced in the pp scattering process at the LHC. In the present paper we limit our discussion to the case in which the gluino is heavier than the squark; for definiteness, we set the SU(3) gaugino mass at the representative value $M_3 = 2 \text{ TeV}$ and the squark soft-mass at the value $m_{\tilde{q}} = 1 \text{ TeV}$. Notice that these two parameters are irrelevant in the specification of the scenarios previously defined.

Many experimental studies are available showing that the production of 1 TeV squarks can be easily discovered at the LHC through inclusive analyses based on the request of a high multiplicity of hard jets and E_T^{miss} , see e.g [3] and [4].

In order to check the supersymmetric model described in the previous sections, the SUSY parameters need to be measured. For this purpose, we employ here a strategy which has been developed for the measurement of the masses of the SUSY particles based on the identification of exclusive decay chains consisting in sequences of two-body decays [3, 16, 17, 18]. The most promising decay chains considered in the literature are:

$$\tilde{q} \rightarrow q\chi_i \rightarrow q\tilde{f}f \rightarrow q\bar{f}f\chi_1 \quad (\text{sequential chain}), \quad (12)$$

and

$$\tilde{q} \rightarrow q\chi_i \rightarrow q(Z, h, H, A)\chi_1 \rightarrow q\bar{f}f\chi_1 \quad (\text{branched chain}), \quad (13)$$

where f stands for a fermion, and the neutralino subscript i can take the values 2, 3 or 4. From the experimental point of view, given the large multiplicity of QCD jets present in pp events, the only interesting decays which can be used for the identification of exclusive chains are the ones involving light charged leptons (e and μ), the hadronic decays of τ (τ -jets) and the fragmentation of b quarks (b -jets), which can be experimentally separated from the background. The sequential chain with two e or μ in the final state is particularly useful, as the whole chain consists of three successive 2-body decays which can be measured very well, and provides enough constraints to allow a model-independent mass determination. The sequential chain with two τ -jets allows a much less clean measurement, as neutrinos are produced in the decay of the τ which make the event kinematic less clear, and a much higher jet background is present. It is however important to detect this chain as well, because by comparing its rate with the rate for the e, μ chain, information can be extracted on the $\tilde{\tau}$ mixing [19]. Finally, the branched chain provides less constraints on the SUSY masses, as the invariant mass of the two final-state fermions just shows a peak at the value of the resonance appearing in the decay. In this case the experimentally interesting decays are the ones in b pairs, especially for the Higgs bosons, and in e and μ for the Z .

These two decay chains have in common the first step consisting in the squark decay $\tilde{q} \rightarrow q\chi_i$. Two types of couplings occur in this process: (a) gauge couplings, universal in the quark flavor, and (b) Yukawa couplings, hierarchical in the quark mass. Gauge (Yukawa) couplings are proportional to the gaugino (Higgsino) components in χ_i , respectively. The actual number of the $q\chi_i$ states produced in a pp collision depends on the product of the cross section for the production process $\sigma(pp \rightarrow \tilde{q}\tilde{q}, \tilde{q}\tilde{q}^*, \tilde{g}\tilde{g}, \tilde{q}\tilde{g})$ times the branching ratio $\text{BR}(\tilde{q} \rightarrow q\chi_i)$. In this product the contribution of the heavy quarks is strongly suppressed, because of their scarcity in the proton composition. Moreover, since the relative importance of the Yukawa couplings as compared to the gauge couplings depends on the ratio m_q/m_Z (m_q and m_Z being the quark mass and the Z -boson mass, respectively) the production of χ_i is more sizable when gauge couplings are effective, i. e. when χ_i has large gaugino components. To account for these properties it is convenient to define an *effective* branching ratio $\text{BR}(\tilde{q} \rightarrow q\chi_i)$, i. e. an average of the branching ratios $\text{BR}(\tilde{q} \rightarrow q\chi_i)$'s over the light quarks [20], including both \tilde{q}_R and \tilde{q}_L . To be conservative, we will use as an effective branching ratio $\text{BR}(\tilde{q} \rightarrow q\chi_i)$ the average over the four lightest quarks. From now on we will simply denote this average as $\text{BR}(\tilde{q} \rightarrow q\chi_i)$.

We turn now to a discussion of the decay process for χ_i , which takes different routes in sequential and branched chains, respectively. In the sequential case, since we have taken $m_{\tilde{q}} = 1$ TeV, the decay can only proceed through a slepton: $\chi_i \rightarrow \tilde{l} \rightarrow \tilde{l}\chi_1$ with a branching ratio $\text{BR}(\chi_i \rightarrow \tilde{l} \rightarrow \tilde{l}\chi_1) = \text{BR}(\chi_i \rightarrow \tilde{l}) \text{BR}(\tilde{l} \rightarrow l\chi_1)$. The size of $\text{BR}(\chi_i \rightarrow \tilde{l})$ depends sensitively on the χ_i composition. If χ_i is dominantly a gaugino, because of the universality of the gaugino couplings, the branching ratios $\text{BR}(\chi_i \rightarrow \tilde{l})$ for the three lepton flavours are about the same; if χ_i is dominantly a Higgsino, χ_i decays predominantly into a $\tilde{\tau}\tau$ pair. In the branched chain χ_i decays either through the Z -boson or through a Higgs boson. The first case, i. e. $\chi_i \rightarrow Z + \chi_1$, involves only the Higgsino components of the two neutralino states; the Z boson subsequently decays into all (kinematically possible) $\tilde{f}f$ pairs according to the Standard Model branching fractions. The second case, i. e. $\chi_i \rightarrow (h, A, H) + \chi_1$, in order to have a sizable BR, requires that one neutralino state is dominantly a gaugino, the other dominantly a Higgsino. Since in our scenarios χ_1 is dominantly a B-ino state, $\chi_i \rightarrow (h, A, H) + \chi_1$ is of interest when χ_i is dominated by the Higgsino components. Because of the hierarchical character of the Yukawa coupling, the subsequent decays of the Higgs bosons are dominated by the production of a $b - \bar{b}$ pair. We note that in the case of a pronounced hierarchical (inverted) scheme (see Fig. 3) the direct $\chi_4 \rightarrow (h, H, A, Z)\chi_1$ decay is suppressed because both χ_4 and χ_1 are dominantly gauginos. This entails that the ‘‘long’’ chains $\chi_4 \rightarrow (h, H, A, Z)\chi_{2,3} \rightarrow (h, H, A, Z)\chi_1$ can give a sizable contribution. Indeed, for both the sequential and branched decays, longer multi-step decay chains, of the type *e.g.* $\chi_4 \rightarrow X\chi_{2,3} \rightarrow XX'\chi_1$, are in principle very interesting as they provide additional kinematic constraints. In practice, the superposition of many decays with the same final state may be extremely difficult to disentangle experimentally, and will thus add confusion rather than information. For this study we will therefore limit ourselves to studying the branching ratio for direct decays.

In the following sections, for the sequential decays we will consider the two cases $f = e, \tau$. We will first analyze e , for which the two chirality states \tilde{e}_R and \tilde{e}_L will be considered separately. The decay $\chi_i \rightarrow e\tilde{e}$ is largely dominated by the gaugino components in χ_i ; thus, if the χ_i decays into both \tilde{e}_R and \tilde{e}_L are kinematically allowed, the ratio of the two branching ratios scales approximately as $BR(\chi_i \rightarrow e\tilde{e}_L)/BR(\chi_i \rightarrow e\tilde{e}_R) \simeq 1/4(1 + \cot\theta a_2^{(i)}/a_1^{(i)})^2$, where $a_2^{(i)}/a_1^{(i)}$ can be approximated by Eqs. (7,8). This implies that χ_i decays dominantly to \tilde{e}_L when it is a pure wino ($a_2^{(i)}/a_1^{(i)} \gg 1$), while either of the two selectron final states $\tilde{e}_{L,R}$ may be important for other compositions. For the τ case we will consider both the mixed (eigenmass) states $\tilde{\tau}_1$ and $\tilde{\tau}_2$. The presence of both states in the decay can be hard to disentangle, and thus make the mass and rate measurements more difficult. For the branched decays we

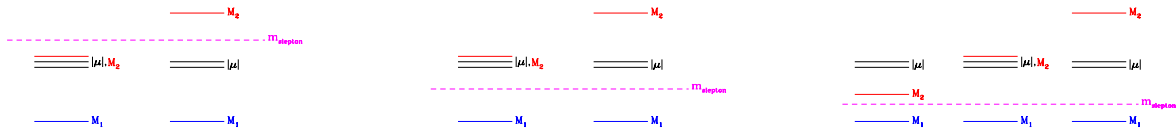


FIG. 4: Qualitative schemes for benchmarks in sequential decay chains: \mathcal{A} -seq1, \mathcal{A} -seq2, \mathcal{B} -seq. For each benchmark, extremes values for M_2 are considered: $M_2 \sim |\mu|$ and $M_2 > |\mu|$ for scenario \mathcal{A} ; $M_2 < |\mu|$, $M_2 \sim |\mu|$ and $M_2 > |\mu|$ for scenario \mathcal{B} .

benchmark	M_1 [GeV]	μ [GeV]	$\tan \beta$	m_A [GeV]	$m_{\tilde{t}}$ [GeV]
\mathcal{A} -seq1	10	110	35	90	150,300,500,700
\mathcal{A} -seq2	10	150	35	90	120
\mathcal{A} -brc	10	110	35	90	150
\mathcal{B} -seq	25	-500	10	1000	120
\mathcal{B} -brc1	25	-500	10	200	120
\mathcal{B} -brc2	25	-500	10	1000	120

TABLE II: Benchmarks for light neutralinos, singled out within the two scenarios \mathcal{A} and \mathcal{B} of Table I. All results will be presented as functions of M_2 , M_2 being varied in the range $100 \text{ GeV} \leq M_2 \leq 1000 \text{ GeV}$. The other supersymmetric parameters are set at the representative values: $M_3 = 2 \text{ TeV}$, $m_{\tilde{q}} = 1 \text{ TeV}$, $A = 0$.

consider the decay into b pairs for the Higgs bosons and the decays into b and e pairs for the Z . In most of the considered models the Z and the SUSY Higgses are almost degenerate, and, given the experimental resolution on the $b\bar{b}$ peak, cannot be separated. It is therefore very useful to have also the decay into leptons, which will allow the experiments to determine the presence of SUSY Higgses in the decay chains.

Based on this discussion, we report our numerical results for all the decay branching ratios relevant for the decay chains of Eqs. (12- 13) in a number of benchmarks within the scenarios \mathcal{A} and \mathcal{B} , previously defined (see Table II). In these benchmarks, all values of the supersymmetric parameters, except M_2 , are fixed. The branching ratios, given as functions of M_2 , have been calculated by using the ISASUSY code[21],

A. Sequential chain benchmarks

In scenario \mathcal{A} the parameter $|\mu|$ is required to be $\mu \sim (100-200) \text{ GeV}$, while slepton masses are unconstrained. On the other hand the sequential chain is sensitive to the hierarchy between $|\mu|$ and $m_{\tilde{t}}$, since, when $m_{\tilde{t}} > |\mu|$, the decay of the $\chi_{2,3}$ states is not allowed by kinematics, and the process (12) can proceed only through χ_4 . On the contrary, when $m_{\tilde{t}} < |\mu|$, the three states χ_i ($i = 2, 3, 4$) take part in the chain (12).

We then fix the following benchmarks for scenario \mathcal{A} :

$$\mathcal{A}\text{-seq1} : \mu = 110 \text{ GeV} \quad m_{\tilde{t}} = 150, 300, 500, 700 \text{ GeV} \quad (14)$$

$$\mathcal{A}\text{-seq2} : \mu = 150 \text{ GeV} \quad m_{\tilde{t}} = 120 \text{ GeV}, \quad (15)$$

where, in both cases, $M_1=10 \text{ GeV}$, $\tan \beta=35$, $m_A =90 \text{ GeV}$ and $A=0$. These two benchmarks are depicted qualitatively in Fig.4 and summarized in Table II.

For the benchmark \mathcal{A} -seq1 the branching ratios for the sequential decay chain are shown in Figs.5,6 where, as already mentioned, only the decay of χ_4 is kinematically allowed. Each panel of the figure corresponds to a different value of $m_{\tilde{t}}$ among those of Eq.(14): $m_{\tilde{t}} =150, 300,500,700 \text{ GeV}$. The notations for the various curves are explained in the figure caption.

The main features of Figs.5 and 6 are readily understood. The Branching Ratio (BR) for $\tilde{q} \rightarrow q\chi_4$ is $\sim 15\%$, since the χ_4 is dominantly wino, and therefore the q_R has no BR into it, and the \tilde{q}_L decays 60% into a chargino χ_2^\pm and 30% into χ_4 , according to the left-handed couplings of the wino. In the regime $M_2 \gg m_{\tilde{t}}$, the χ_4 decays with 40% BR into W , Z and Higgses because of its non-zero Higgsino component, 60% BR into the left-handed sleptons. So

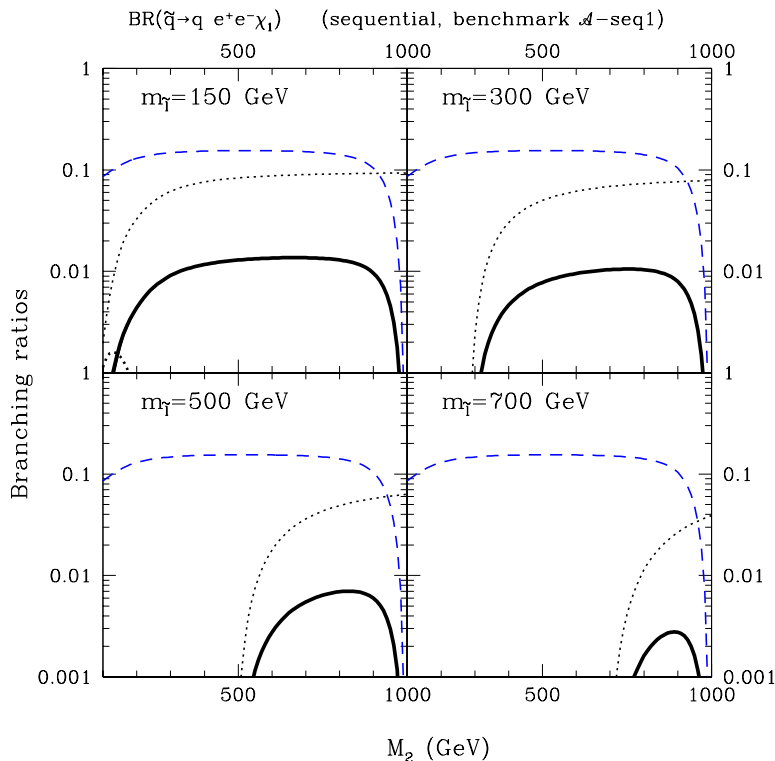


FIG. 5: Branching ratios for the sequential process $\tilde{q} \rightarrow \bar{e}e\chi_1$ in benchmark \mathcal{A} -seq1 as functions of M_2 . Each panel corresponds to a different value of $m_{\tilde{\tau}}$. The dashed lines show the branching ratio for the process $\tilde{q} \rightarrow q\chi_4$; the thin-dotted lines denote the branching ratio for the process $\chi_4 \rightarrow e\tilde{e}_L \rightarrow e\bar{e}\chi_1$; the thick-dotted line in the top-left panel denotes the branching ratio for the process $\chi_4 \rightarrow e\tilde{e}_R \rightarrow e\bar{e}\chi_1$ (the corresponding curves cannot be seen in the other panels because they are too low); the thick solid lines denote the branching ratio for the whole sequential decay chain $\tilde{q} \rightarrow q\chi_4 \rightarrow qe\bar{e} \rightarrow qe\bar{e}\chi_1$.

for \tilde{e}_L the BR is $\sim 10\%$. For each of the two $\tilde{\tau}$ states, which are in this case rather similar in composition and mass, the BR is $\sim 5\%$ for each state. For instance, for $m_{\tilde{\tau}} = 150$ GeV: $m_{\tilde{\tau}_1} = 133$ GeV, $m_{\tilde{\tau}_2} = 176$ GeV and for $m_{\tilde{\tau}} = 300$ GeV: $m_{\tilde{\tau}_1} = 192$ GeV, $m_{\tilde{\tau}_2} = 314$ GeV.

The different quadrants of Figs. 5 and 6 show by how much the branching ratios are suppressed for growing values of $m_{\tilde{\tau}}$, due to the reduction of the available phase space for the decay $\chi_4 \rightarrow \tilde{l}\bar{l}$. On the other hand, a growing value of $m_{\tilde{\tau}}$ does not affect $BR(\tilde{l} \rightarrow l\chi_1)$, which is very close to 1 in all cases. Note that in this benchmark whenever $M_2 \gtrsim |\mu|$ one has $m_{\chi_4} \sim M_2$, thus a measurement of m_{χ_4} would typically give direct access to the value of M_2 .

The phenomenology of the sequential decay becomes richer in the benchmark \mathcal{A} -seq2, which is shown in Figs.7 and 8. In fact in this case the process (12) can proceed through the production and decay of any of the χ_i states. The corresponding separate contributions to the decay branching ratios for $i = 2, 3, 4$ are shown in each of the first three panels of Figs.7 and 8 while the last panel shows the combined total branching ratios.

The branching ratios for the process $\tilde{q} \rightarrow q\chi_4$, shown in the bottom-left panel of Figs.7-8, are obviously very similar the ones already displayed in Figs.5-6, and previously commented. As compared to these, the branching ratios for the processes $\tilde{q} \rightarrow q\chi_i$ ($i = 2, 3$) are somewhat suppressed, due to the prevalent Higgsino compositions of χ_2, χ_3 . For the same reason, the BR of χ_2 and χ_3 into $e_{L,R}$, is at most a couple of percent. The contrary happens for the branching ratios $BR(\chi_i \rightarrow \tilde{\tau}\tau\chi_1)$. In this case χ_2, χ_3 decay into $\tilde{\tau}\tau$ with larger BRs than χ_4 , because the dominance of the Higgsino components in χ_2, χ_3 favors their decays into third generation leptons. Notice that in the case of χ_2 , only the lighter stau contributes, since $\tilde{\tau}_2$ is heavier than χ_2 ; in the case of χ_3 , the $\tilde{\tau}_2$ contribution is very strongly suppressed as

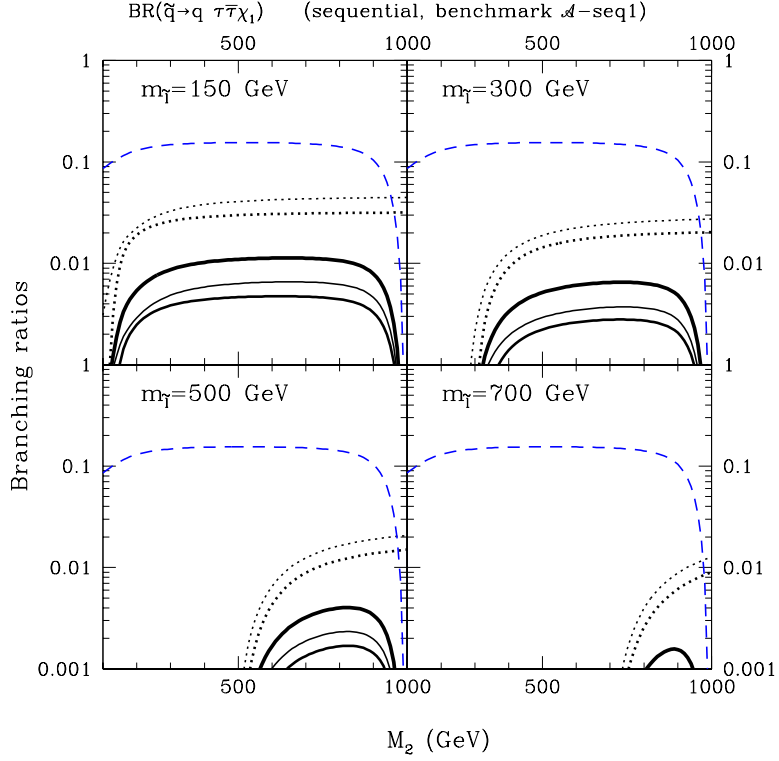


FIG. 6: Branching ratios for the sequential process $\tilde{q} \rightarrow \tilde{\tau}\tau\chi_1$ in benchmark \mathcal{A} -seq1 as functions of M_2 . Each panel corresponds to a different value of $m_{\tilde{\tau}}$. The dashed lines show the branching ratio for the process $\tilde{q} \rightarrow q\chi_4$; the thin-dotted lines denote the branching ratio for the process $\chi_4 \rightarrow \tau\tilde{\tau}_1 \rightarrow \tau\tilde{\tau}\chi_1$; the thick-dotted lines denote the branching ratio for the process $\chi_4 \rightarrow \tau\tilde{\tau}_2 \rightarrow \tau\tilde{\tau}\chi_1$; the thin-solid lines denote the branching ratio for the whole sequential decay chain $\tilde{q} \rightarrow q\chi_4 \rightarrow q\tau\tilde{\tau}_1 \rightarrow q\tau\tilde{\tau}\chi_1$; the solid lines with intermediate thickness denote the branching ratio for the whole sequential decay chain $\tilde{q} \rightarrow q\chi_4 \rightarrow q\tau\tilde{\tau}_2 \rightarrow q\tau\tilde{\tau}\chi_1$; the thickest solid lines denote the total branching ratio for the whole sequential decay chain $\tilde{q} \rightarrow q\chi_4 \rightarrow q\tau\tilde{\tau} \rightarrow q\tau\tilde{\tau}\chi_1$.

compared to the $\tilde{\tau}_1$ contribution again for phase-space reasons. All in all, in the full process $\tilde{q} \rightarrow q\chi_i \rightarrow q\tilde{\tau} \rightarrow q\tau\tilde{\tau}\chi_1$, the most relevant contribution turns out to be provided by χ_2 .

The scenario \mathcal{B} is characterized by a heavy pseudoscalar Higgs mass ($m_A \gtrsim 200$ GeV) and by a very light stau, which is required in order to keep the neutralino relic abundance below the observational limit. Moreover, as explained in Section II B, $|\mu|$ must be large. We define in this case the following benchmark, corresponding to the lightest possible mass of the neutralino χ_1 :

$$\begin{aligned} \mathcal{B}\text{-seq} : \quad M_1 &= 25 \text{ GeV} & \mu &= -500 \text{ GeV} & \tan\beta &= 10 \\ m_{\tilde{\tau}} &= 87 \text{ GeV} & (m_{\tilde{\tau}} &= 120 \text{ GeV}) & A &= 0. \end{aligned} \quad (16)$$

This benchmark is depicted qualitatively in Fig.4 and summarized in Table II. The branching ratios for this benchmark are shown in Figs. 9–10. In this case the possible hierarchy between M_2 and $|\mu|$ is richer than in the previous benchmark \mathcal{A} -seq1, since now also $M_2 \ll |\mu|$ can occur. In particular, this implies that the compositions of χ_2 and χ_4 flip the one into the other in going from $M_2 < |\mu|$ to $M_2 > |\mu|$ (an example of this behaviour can be seen in Fig.2, although for a slightly different set of supersymmetric parameters). Here, for $M_2 < 500$ GeV, χ_2 is mainly a gaugino, whereas χ_4 is dominantly a Higgsino; the other way around, for $M_2 > 500$ GeV. While χ_2 and χ_4 exchange their roles as M_2 runs over its range, χ_3 is steadily a Higgsino, independently of M_2 . On the basis of these properties one understands

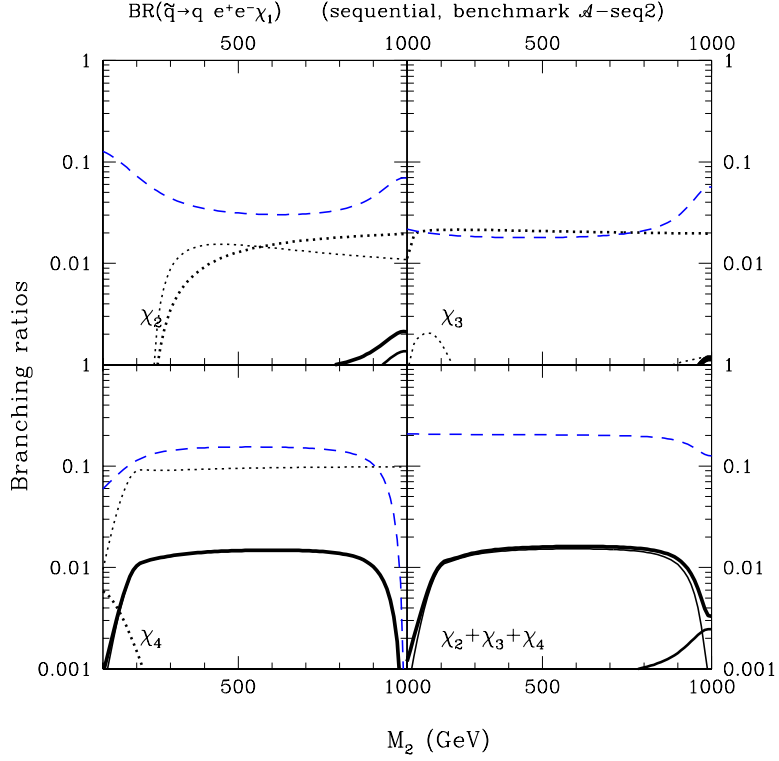


FIG. 7: Branching ratios for the sequential process $\tilde{q} \rightarrow \bar{e}e\chi_1$ in benchmark \mathcal{A} -seq2 as functions of M_2 . Each of the first three panels corresponds to a different intermediate neutralino state ($\chi_i, i = 2, 3, 4$) in the sequential chain, while the last panel refers to combined branching ratios. The dashed lines show the branching ratio for the process $\tilde{q} \rightarrow q\chi_4$; the thin-dotted lines denote the branching ratio for the process $\chi_4 \rightarrow e\bar{e}_L \rightarrow e\bar{e}\chi_1$; the thick-dotted lines denote the branching ratio for the process $\chi_4 \rightarrow e\bar{e}_R \rightarrow e\bar{e}\chi_1$. The thin-solid lines denote the branching ratio for the whole sequential decay chain $\tilde{q} \rightarrow q\chi_4 \rightarrow qe\bar{e}_L \rightarrow qe\bar{e}\chi_1$; the solid-lines with intermediate thickness denote the branching ratio for the whole sequential decay chain $\tilde{q} \rightarrow q\chi_4 \rightarrow qe\bar{e}_R \rightarrow qe\bar{e}\chi_1$; the thickest solid lines denote the total branching ratio for the whole sequential decay chain $\tilde{q} \rightarrow q\chi_4 \rightarrow qe\bar{e} \rightarrow qe\bar{e}\chi_1$ (some curves do not appear in all panels because they are too low).

the features of the branching ratios for the production of the χ_i intermediate states (dashed lines). It is also clear why their combined results (dashed line in the bottom-right panel) have a much milder dependence on M_2 .

As for the peculiar behaviour of the branching ratios for the decays $\chi_i \rightarrow l\bar{l}\chi_1$ (dotted lines), notice that their sudden drop at low M_2 in the cases of χ_3 and χ_4 is due to the opening of some competing decay channels. In fact, for $M_2 < |\mu|$ one has $m_3 \simeq m_4 \simeq |\mu|$ and, at the same time, the chargino mass is of order M_2 . Thus, under these circumstances, χ_3 and χ_4 have a sizable branching ratio into a chargino- W state ($\sim 54\%$ at $M_2 = 300$ GeV). In addition, also the channel $\chi_3 \rightarrow \chi_2 Z$ becomes important in this case (with a branching ratio of about 22% at $M_2 = 300$ GeV).

B. Branched chain benchmarks

In the branched chains the decay amplitude is sensitive to the value of m_A , while it does not depend on $m_{\tilde{l}}$. As a consequence of this, as far as scenario \mathcal{A} is considered, for branched decays we adopt the following benchmark:

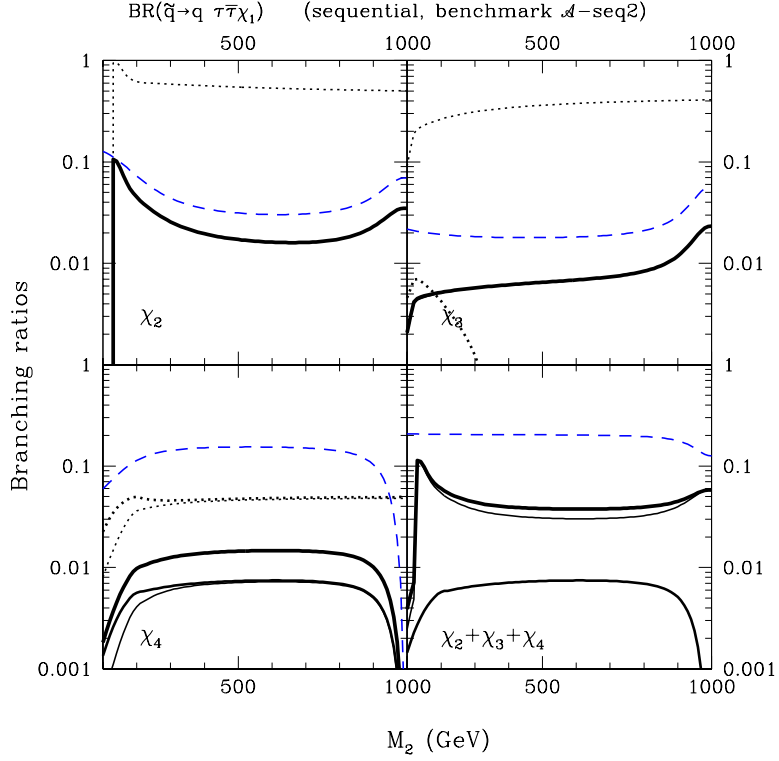


FIG. 8: Branching ratios for the sequential process $\tilde{q} \rightarrow \tilde{\tau}\tau\chi_1$ in benchmark \mathcal{A} -seq2 as functions of M_2 . Each of the first three panels corresponds to a different intermediate neutralino state ($\chi_i, i = 2, 3, 4$) in the sequential chain, while the last panel refers to combined branching ratios. The codes for the various curves are as in Fig. 6.

$$\begin{aligned} \mathcal{A}\text{-brc} : M_1 = 10 \text{ GeV} \quad \mu = 110 \text{ GeV} \\ \tan\beta = 35 \quad m_A = 90 \text{ GeV} \quad A = 0, \end{aligned} \quad (17)$$

while the value of $m_{\tilde{l}}$ is undetermined (for definiteness, in this case we fix $m_{\tilde{l}} = 150 \text{ GeV}$). This benchmark is depicted qualitatively in Fig.11 and summarized in Table II. The branching ratios for benchmark \mathcal{A} -brc are displayed in Fig.12, where the dotted lines show the branching ratio for the process $\chi_i \rightarrow Z\chi_1$, the short-dashed lines correspond to the process $\chi_i \rightarrow h\chi_1$, the long-dashed lines indicate the process $\chi_i \rightarrow H\chi_1$, the dot-dashed lines denote the process $\chi_i \rightarrow A\chi_1$ and, finally, the solid line indicates the combined branching ratio for the whole decay chain $\tilde{q} \rightarrow q\chi_i \rightarrow q(Z, h, H, A)\chi_1 \rightarrow q\bar{b}\bar{b}\chi_1$. Note that in this Figure the branching ratios for the process $\tilde{q} \rightarrow q\chi_i$, already displayed in Figs. 5,6 for the same set of parameters, are omitted. The combined branching ratio for the decay $\tilde{q} \rightarrow q\chi_i \rightarrow qZ\chi_1 \rightarrow qe^+e^-\chi_1$, to which only the Z exchange contributes, can be simply calculated by scaling the line for Z by a factor 0.22, the ratio of $BR(Z \rightarrow e^+e^-)$ and $BR(Z \rightarrow \bar{b}b)$ in the Standard Model.

As shown in Fig.12, the major contribution to the branching ratio $BR(\tilde{q} \rightarrow \bar{b}\bar{b}\chi_1)$ is due to the production of χ_2 , which subsequently decays into χ_1 through the production of a Z boson or a A Higgs boson, provided $|m_2|$ is above threshold (which implies that $M_2 \gtrsim 150 \text{ GeV}$). These two channels have large branching ratios, due to the fact that χ_2 is mainly a Higgsino, and also χ_1 has a sizable Higgsino component. The branching ratio of the channel through Z prevails over the branching ratio of the channel through A roughly by a factor 4, since a factor 7-10 due to the Lorentz structure of the matrix elements is partially compensated by a factor 0.7-0.5 due to the different coupling constants.

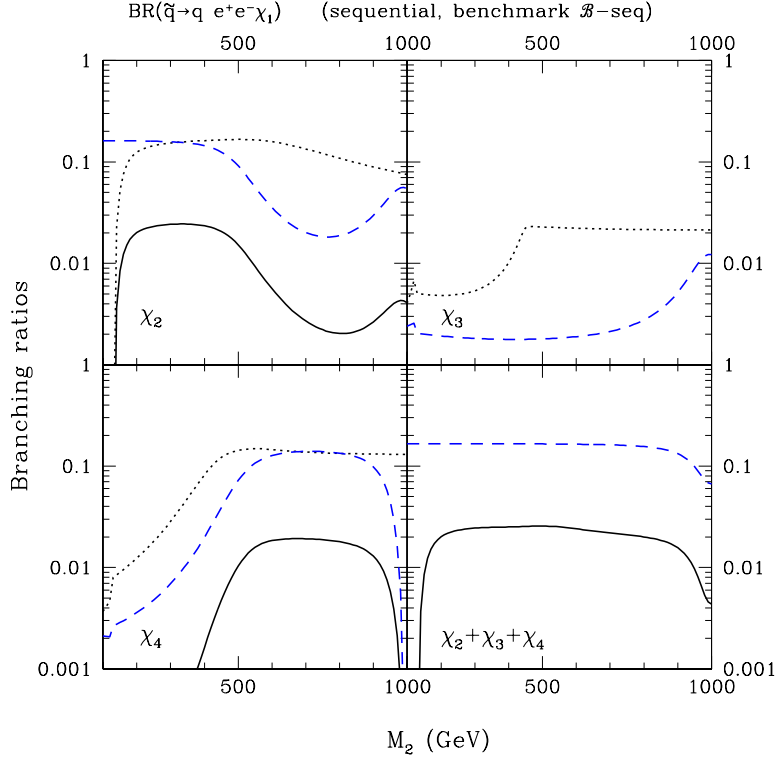


FIG. 9: Branching ratios for the sequential process $\tilde{q} \rightarrow \bar{e}e\chi_1$ in benchmark \mathcal{B} -seq as functions of M_2 . Notations are as in Fig.7.

As far as branched decays are concerned, the most relevant feature of the scenario \mathcal{B} is that m_A is heavy ($m_A \gtrsim 200$ GeV), while $\tan\beta \lesssim 10$ is moderate. As a consequence of this, lower branching ratios are expected compared to the previous case of benchmark \mathcal{A} -brc. In scenario \mathcal{B} we adopt the two following benchmarks:

$$\mathcal{B}\text{-brc1} : m_A = 200 \text{ GeV} \quad (18)$$

$$\mathcal{B}\text{-brc2} : m_A = 1000 \text{ GeV}, \quad (19)$$

where, in both cases, $\mu = -500$ GeV, $M_1=25$ GeV, $\tan\beta=10$, $m_{\tilde{l}} = 120$ GeV and $A = 0$. These benchmarks are depicted qualitatively in Fig.11 and summarized in Table II. The corresponding branching ratios are shown in Figs.13 and 14. Note that in Fig.14 only the decays $\chi_i \rightarrow Z\chi_1$ and $\chi_i \rightarrow h\chi_1$ are kinematically allowed. The main features of these figures may readily be accounted for by arguments similar to the ones previously described.

C. Expected number of events

In order to assess the experimental detectability of our scenarios, we now display in Figs.15 – 17 the total production cross sections for the process $pp \rightarrow X f \bar{f} \chi_1$ with $\sqrt{s} = 14$ TeV for each of the benchmarks previously introduced ($f = \tau$ and $f = e$, for the cases \mathcal{A} -seq1, \mathcal{A} -seq2 and \mathcal{B} -seq, are displayed in Fig. 15 and in Fig. 16, respectively; $f = b$, for the cases \mathcal{A} -brc, \mathcal{B} -brc1 and \mathcal{B} -brc2, is displayed in Fig. 17). Notice that the case $f = e$ for branched chains can simply be derived by scaling the lines of the top-left panel of Fig. 17 (production of a Z -boson) by a factor 0.22, the ratio of $BR(Z \rightarrow e^+e^-)$ and $BR(Z \rightarrow b\bar{b})$ in the Standard Model.

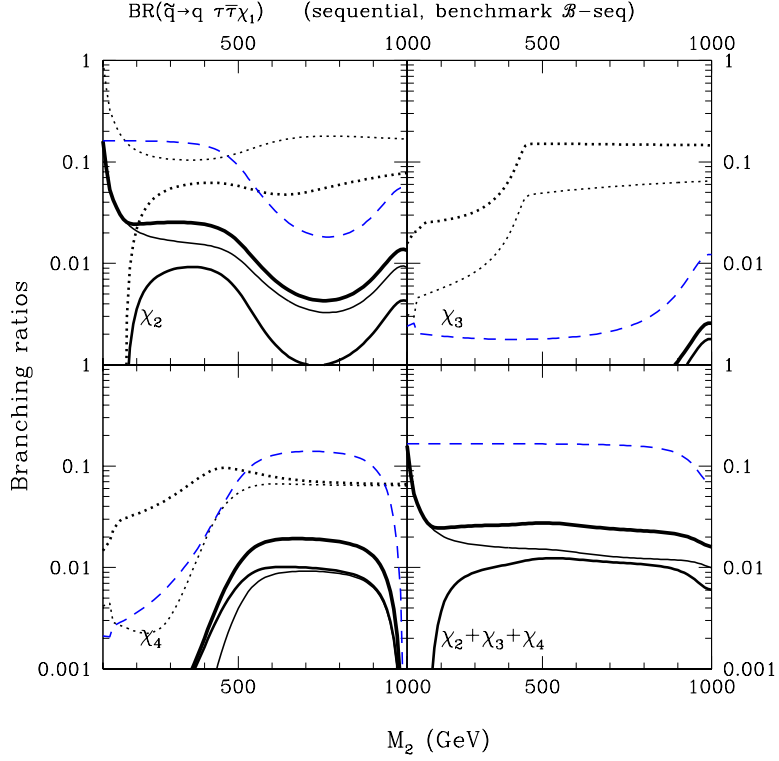


FIG. 10: Branching ratios for the sequential process $\tilde{q} \rightarrow \bar{\tau}\tau\chi_1$ in benchmark \mathcal{B} -seq as functions of M_2 . Notations are as in Fig.6.

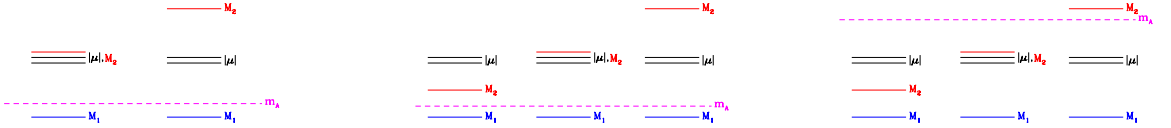


FIG. 11: Qualitative schemes of benchmarks for branched decay chains: \mathcal{A} -brc, \mathcal{B} -brc1, \mathcal{B} -brc2. For each benchmark, extremes values for M_2 are considered: $M_2 \sim |\mu|$ and $M_2 > |\mu|$ for scenario \mathcal{A} ; $M_2 < |\mu|$, $M_2 \sim |\mu|$ and $M_2 > |\mu|$ for scenario \mathcal{B} .

A rough estimate of the expected events after two year's high-luminosity running at LHC is indicated on the vertical axis on the right of these figures. For the calculation of the production cross sections $\sigma(pp \rightarrow \tilde{q}\tilde{q}, \tilde{q}\tilde{q}^*, \tilde{g}\tilde{g}, \tilde{q}\tilde{g})$ we have used the code PROSPINO [22]

We assume here arbitrarily that the cuts required to extract the SUSY signal from the background will have an efficiency of the order of 10%, and a reasonably precise measurement can be performed for a chain for which ~ 100 events are left after the experimental cuts.

From the results summarized in Figs.15 – 17 it turns out that there are very good perspectives for a fruitful investigation of the supersymmetric parameter space relevant for light neutralinos at LHC. In particular we notice that: 1) The scenario \mathcal{A} should be easily explorable both through sequential decay chains and through branched chains. 2) For the sequential case good perspectives are offered by the $\bar{e}e$ signal and by the $\bar{\tau}\tau$ one in both benchmarks \mathcal{A} -seq1 and \mathcal{A} -seq2. In particular, notice that in the benchmark \mathcal{A} -seq1 the $\bar{e}e$ and the $\bar{\tau}\tau$ signals are about of the same size, because they take origin from the decay of χ_4 , which for $M_2 > |\mu|$ is dominantly a gaugino; on the

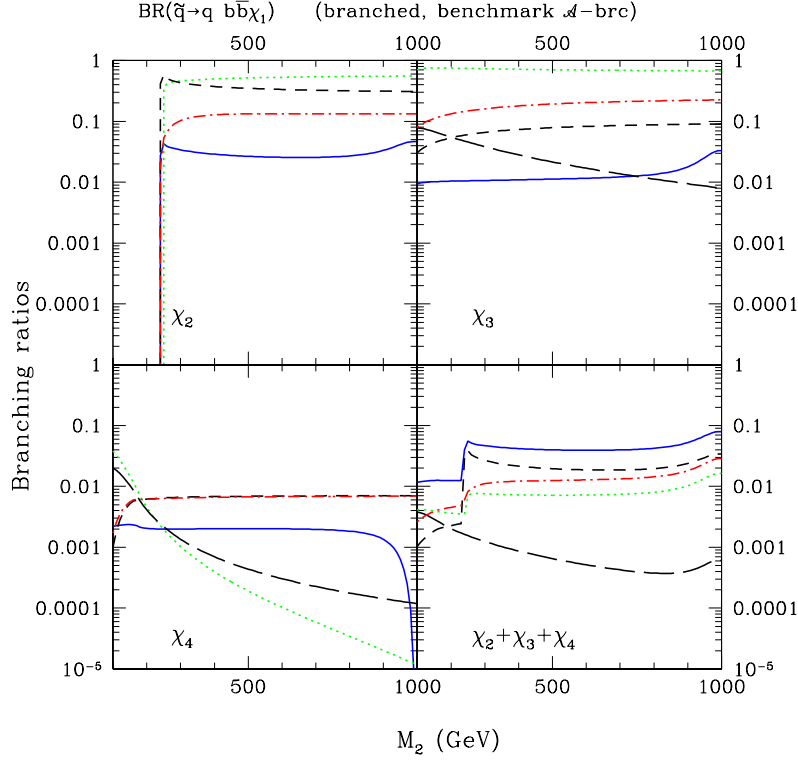


FIG. 12: Branching ratios for the branched chain in benchmark \mathcal{A} -brc as functions of M_2 . Each of the first three panels corresponds to a different intermediate neutralino state ($\chi_i, i = 2, 3, 4$) in the branched chain, while the last panel provides the branching ratios summed over all χ_i 's. Notations are as follows. Dotted lines: branching ratio for the process $\chi_i \rightarrow Z\chi_1$; short-dashed lines: branching ratio for the process $\chi_i \rightarrow h\chi_1$; long-dashed lines: branching ratio for the process $\chi_i \rightarrow H\chi_1$; dot-dashed lines: branching ratio for the process $\chi_i \rightarrow A\chi_1$; solid line: combined branching ratios for the whole decay chain $\tilde{q} \rightarrow q\chi_i \rightarrow q(Z, h, H, A)\chi_1 \rightarrow qbb\chi_1$. The branching ratios for the process $\tilde{q} \rightarrow q\chi_i$, already displayed in Figs. 7,8, are omitted here.

contrary, in the benchmark \mathcal{A} -seq2 the $\bar{\tau}\tau$ signal is larger than the $\bar{e}e$ one, since in this case the process goes mainly through intermediate Higgsino-like neutralino states. 3) For the branched case the scenario \mathcal{A} gives good measurement perspectives for production of a $\bar{b}b$ pair through Z and h, A Higgs bosons. 4) In scenario \mathcal{B} large signals are expected in terms of $\bar{e}e$ and $\bar{\tau}\tau$ pairs in sequential processes; these two signals are comparable in size, since they are generated by intermediate neutralino states which are dominantly gauginos. 5) Higher statistics will be required to explore the scenario \mathcal{B} by branched decay; the most favorable processes are represented by those mediated by Z or h, A Higgs bosons when $M_2 > |\mu|$.

The rates are of course function of the assumed squark mass of 1 TeV. Since the BR for the considered chains do not depend on the squark mass, results for different squark masses can be obtained by scaling down the curves by the relative squark production cross-section. As the squark mass gets nearer to the gluino mass a significant contribution will also come from squarks produced in gluino decays. For instance for a gluino mass of 2 TeV and a squark mass of $\sim 1500(1900)$ GeV, the scaling factor would be respectively $\sim 6(25)$, and the fraction of events with at least a gluino in the initial state would be respectively $\sim 18\%(55\%)$.

We stress that here our considerations are simply based on the evaluated total number of events. The actual potentiality of investigation at LHC of the present signals will require a detailed analysis in terms of signal to background ratios and specific kinematical distributions. This further investigation is beyond the scope of this paper

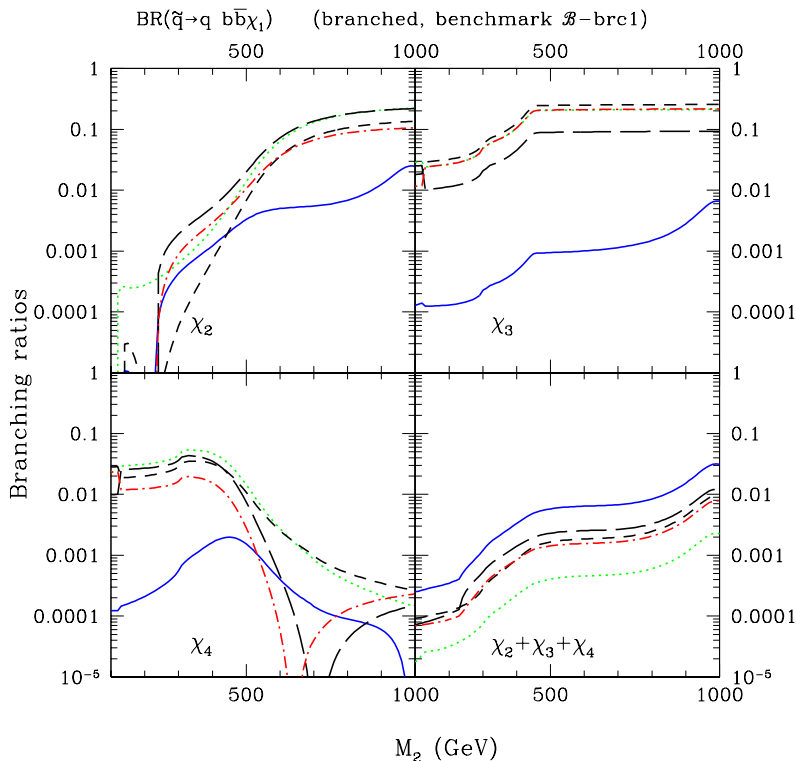


FIG. 13: Branching ratios for the branched chain in benchmark \mathcal{B} -brc1 as functions of M_2 . Notations are as in Fig.12. The branching ratios for the process $\tilde{q} \rightarrow q\chi_i$, already displayed in Figs. 9,10, are omitted here.

and will be presented elsewhere [23].

V. CONCLUSIONS

In this paper we have analyzed the discovery potential of LHC with respect to light neutralinos, *i.e.* neutralinos with a mass $m_\chi \lesssim 50$ GeV, which arise in supersymmetric models where gaugino masses are not unified at a Grand Unified (GUT) scale. These neutralinos have been thoroughly investigated in Refs. [1, 2], under the hypotheses that R-parity is conserved and that the lowest neutralino state is the Lightest Supersymmetric Particle (LSP). This LSP light neutralino has been proved to be quite interesting as a cold dark matter particle intervening in a number of direct and indirect astrophysical effects.

In particular, in Refs. [1, 2] it was derived that the present constraints due to accelerator and other precision measurements, together with limits imposed by cosmological observations, concur in confining these neutralinos to configurations located in a well delimited part of the supersymmetric parameter space. In other words, the relevant region of the SUSY parameter space can be described by a limited number of free parameters, since some of the model parameters are essentially frozen by the external constraints.

Such a situation implies that a few scenarios and relevant conspicuous benchmarks can naturally be singled out. This is the strategy that we have used in the present paper in order to explore the discovery potential of LHC as far as light neutralinos are concerned.

The simplicity of the underlying supersymmetric model also allows the derivation of analytic formulae which help a lot in understanding the main properties of the spectroscopy of the four neutralino states. The relevant expressions

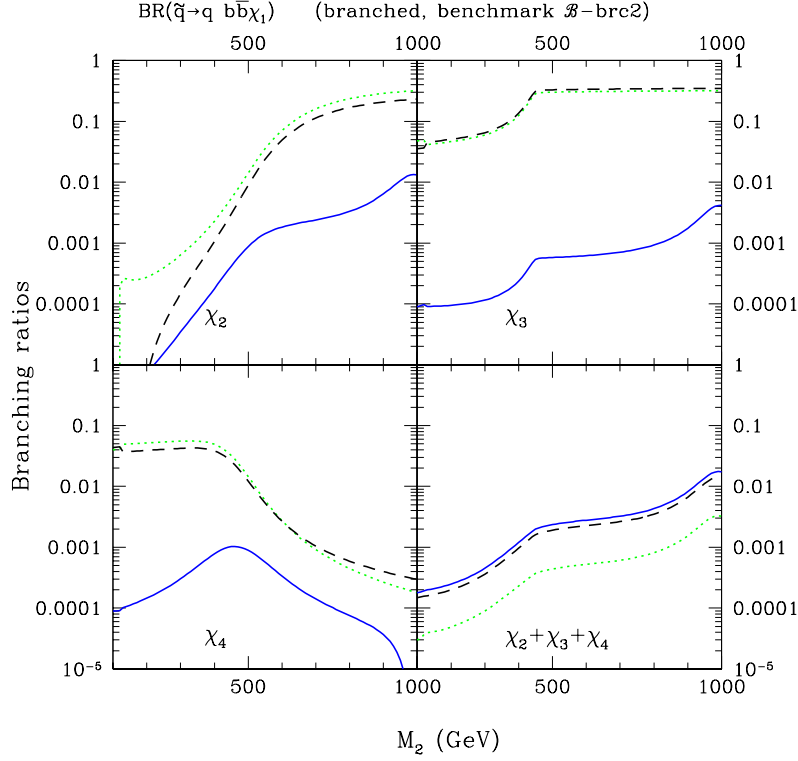


FIG. 14: Branching ratios for the branched chain in benchmark \mathcal{B} -brc2 as functions of M_2 . Notations are as in Fig.12. The branching ratios for the process $\tilde{q} \rightarrow q\chi_i$, already displayed in Figs. 9,10, are omitted here.

have been derived in the first part of the paper.

Two main scenarios have been introduced: the scenario \mathcal{A} , where the stable neutralino has a mass $m_\chi \sim 10$ GeV, and the scenario \mathcal{B} where $m_\chi \sim 25$ GeV (the specification for the values of the other supersymmetric parameters is given in Table I). Within these two scenarios a number of convenient benchmarks have been introduced (see Table II).

In the framework of the selected benchmarks we have considered the following decay chains, generated by squarks produced in the proton–proton scattering: $\tilde{q} \rightarrow q\chi_i \rightarrow q\tilde{f}f \rightarrow q\tilde{f}f\chi_1$ (sequential chain), and $\tilde{q} \rightarrow q\chi_i \rightarrow q(Z, h, H, A)\chi_1 \rightarrow q\tilde{f}f\chi_1$ (branched chain). We limited our discussion to the case in which the gluino is heavier than the squark; for definiteness, we have set the SU(3) gaugino mass at the representative value $M_3 = 2$ TeV and the squark soft-mass at the value $m_{\tilde{q}} = 1$ TeV. Notice that these two parameters are irrelevant in the specification of our scenarios inspired by cosmology.

Branching ratios and number of events expected at LHC have been evaluated for the signals which proved to be the most important ones for experimental investigation.

We arrived at the following main conclusions:

i) The scenario \mathcal{A} should be easily explorable both through sequential decay chains and through branched chains. For the sequential case good perspectives are offered by the $\bar{e}e$ (or $\bar{\mu}\mu$) signal and by the $\bar{\tau}\tau$ one. For the branched case the scenario \mathcal{A} gives good measurement perspectives for production of a $\bar{b}b$ pair through Z and h, A Higgs bosons, combined with light lepton pairs through Z.

ii) In scenario \mathcal{B} large signals are expected in terms of $\bar{e}e$ (or $\bar{\mu}\mu$) and $\bar{\tau}\tau$ pairs in sequential processes. High statistics will be required to explore the scenario \mathcal{B} by branched decay; the most favorable processes being represented by those mediated by Z or h, A Higgs bosons when $M_2 > |\mu|$.

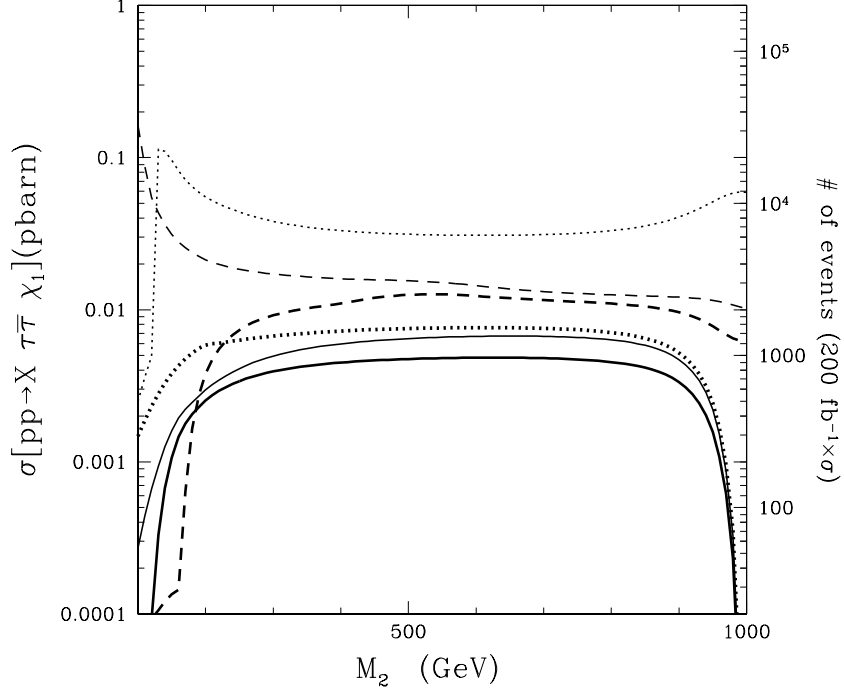


FIG. 15: Total production cross sections for the processes $pp \rightarrow X\tau\bar{\tau}\chi_1$ in the benchmarks for sequential chains for $\sqrt{s} = 14$ TeV, as functions of M_2 . The decay branching ratios included in the calculation are those displayed in Figs. 6,8,10. The notation is as follows. Thin–solid line: \mathcal{A} –seq1 with $m_{\tilde{t}} = 150$ GeV and mediation of $\tilde{\tau}_1$; thick–solid line: \mathcal{A} –seq1 with $m_{\tilde{t}} = 150$ GeV and mediation of $\tilde{\tau}_2$; thin–dotted line: \mathcal{A} –seq2 with mediation of $\tilde{\tau}_1$; thick–dotted line: \mathcal{A} –seq2 with mediation of $\tilde{\tau}_2$; thin–dashed line: \mathcal{B} –seq with mediation of $\tilde{\tau}_1$; thick–dashed line: \mathcal{B} –seq with mediation of $\tilde{\tau}_2$. On the right vertical axis the corresponding total number of expected events is shown, assuming a luminosity of 200 fb^{-1} (two years of high–luminosity run at LHC).

These results show that LHC has a strong potential in the investigation of the supersymmetric parameter region compatible with a light neutralino. Due to the characteristic features of this region, the measurements of LHC should easily prove or disprove our model.

Finally, we wish to recall that our conclusions are based on the evaluated total number of events, only. To ascertain the actual potentiality of LHC in the study of our model, the investigation has to be pursued to include analysis of the signal/background ratios and of specific kinematical distributions. This further investigation will be presented in a subsequent publication [23].

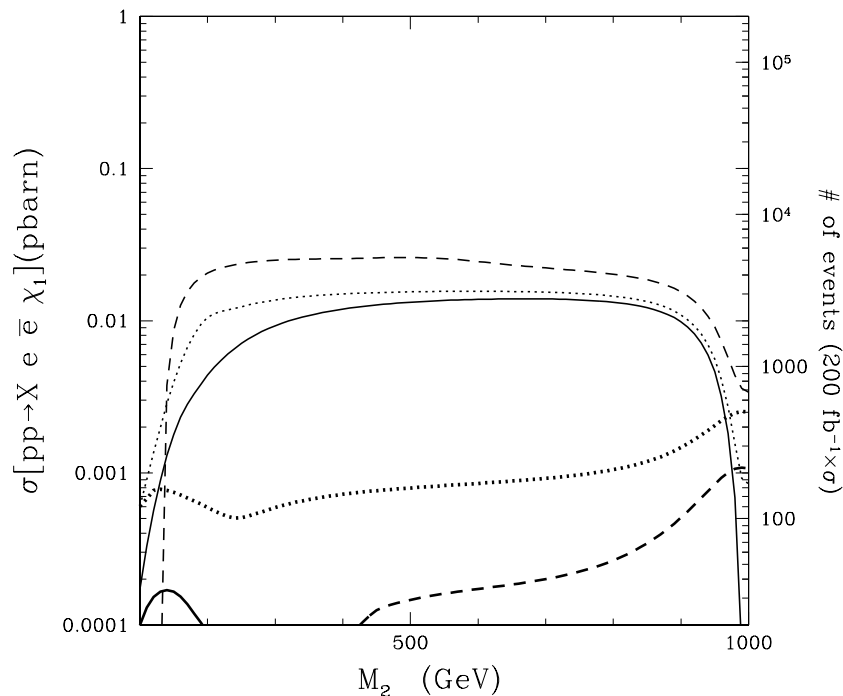


FIG. 16: Total production cross sections for the processes $pp \rightarrow X e \bar{e} \chi_1$ in the benchmarks for sequential chains for $\sqrt{s} = 14$ TeV, as functions of M_2 . The decay branching ratios included in the calculation are those displayed in Figs. 5,7,9. The notation is as follows. Thin-solid line: \mathcal{A} -seq1 with $m_{\tilde{t}} = 150$ GeV and mediation of \tilde{e}_L ; thick-solid line: \mathcal{A} -seq1 with $m_{\tilde{t}} = 150$ GeV and mediation of \tilde{e}_R ; thin-dotted line: \mathcal{A} -seq2 with mediation of \tilde{e}_L ; thick-dotted line: \mathcal{A} -seq2 with mediation of \tilde{e}_R ; thin-dashed line: \mathcal{B} -seq with mediation of \tilde{e}_L ; thick-dashed line: \mathcal{B} -seq with mediation of \tilde{e}_R . On the right vertical axis the corresponding total number of expected events is shown, assuming a luminosity of 200 fb^{-1} (two years of high-luminosity run at LHC).

Acknowledgments

We acknowledge Research Grants funded jointly by Ministero dell'Istruzione, dell'Università e della Ricerca (MIUR), by Università di Torino and by Istituto Nazionale di Fisica Nucleare within the *Astroparticle Physics Project*.

-
- [1] A. Bottino, N. Fornengo and S. Scopel, Phys. Rev. D **67**, 063519 (2003) ; A. Bottino, F. Donato, N. Fornengo and S. Scopel, Phys. Rev. D **68**, 043506 (2003).
 - [2] A. Bottino, F. Donato, N. Fornengo and S. Scopel: Phys. Rev. D **69**, 037302 (2004); Phys. Rev. D **70**, 015005 (2004) and Phys. Rev. D **77**, 015002 (2008).
 - [3] ATLAS Collaboration, *ATLAS detector and physics performance Technical Design Report*, CERN/LHCC 99-14/15 (1999). <http://atlas.web.cern.ch/Atlas/GROUPS/PHYSICS/TDR/access.html>.
 - [4] CMS Collaboration *CMS physics : Technical Design Report v.2 : Physics performance* CERN-LHCC-2006-021 (2006). <http://cdsweb.cern.ch/search.py?recid=942733>.
 - [5] A. Colaleo (ALEPH Collaboration), talk at SUSY'01, June 11-17, 2001, Dubna, Russia; J. Abdallah et al. (DELPHI Collaboration), DELPHI 2001-085 CONF 513, June 2001; LEP Higgs Working Group for Higgs boson searches,

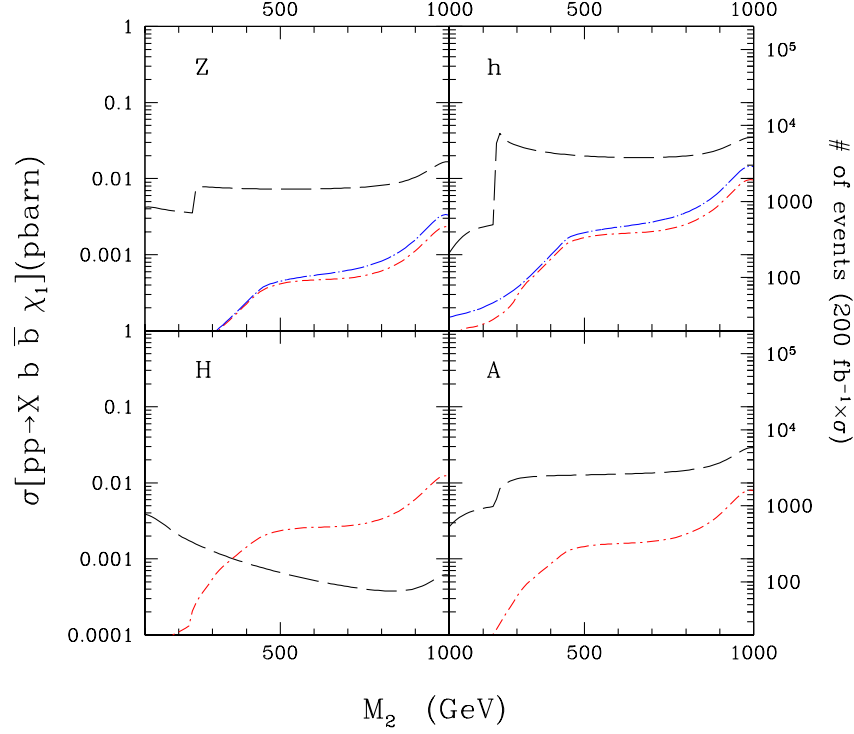


FIG. 17: Total production cross sections for the processes $pp \rightarrow X b \bar{b} \chi_1$ in the benchmarks for branched chains, discussed in the text, and for $\sqrt{s} = 14$ TeV, as functions of M_2 . The decay branching ratios included in the calculation are those displayed in Figs. 12–14. The top-left panel refers to the production of a Z -boson, the top-right panel to the production of an h -boson, the bottom-left panel to the production of an H -boson, and the bottom-right panel to the production of an A -boson. The notation for the curves is as follows. Long-dashed line: \mathcal{A} -brc; dot-short dashed line: \mathcal{B} -brc1; dot-long dashed line: \mathcal{B} -brc2. On the right vertical axis the corresponding total number of expected events is shown, assuming a luminosity of 200 fb^{-1} (two years of high-luminosity run at LHC).

arXiv:hep-ex/0107029; LEP2 Joint SUSY Working Group, <http://lepsusy.web.cern.ch/lepsusy/>.

- [6] A.A. Affolder *et al.* (CDF Collaboration), Phys. Rev. Lett. **86**, 4472 (2001); V.M. Abazov *et al.* (D0 Collaboration), Phys. Rev. Lett. **97**, 171806 (2006).
- [7] E. Barberio *et al.* (HFAG), arXiv:hep-ex/0603003.
- [8] M. Ciuchini, G. Degrassi, P. Gambino and G.F. Giudice, Nucl. Phys. B **534**, 3 (1998).
- [9] M. Misiak *et al.*, Phys. Rev. Lett. **98**, 022002 (2007).
- [10] V.M. Abazov *et al.*, (D0 Collaboration), Phys. Rev. D **76**, 092001 (2007).
- [11] G.W. Bennet *et al.* (Muon g-2 Collaboration), Phys. Rev. D **73**, 072003 (2006).
- [12] J. Bijnens and J. Prades, Mod. Phys. Lett. A **22**, 767 (2007).
- [13] The first of Eqs. (4) is also derived in M. M. El Kheishen, A. A. Shafik and A. A. Aboshousha, Phys. Rev. D **67**, 4345 (1992).
- [14] D.N. Spergel *et al.*, Astrophys. J. Suppl. Ser. **148**, 175 (2003); M. Tegmark *et al.*, Phys. Rev. D **69**, 103501 (2004).
- [15] This lower limit is also found in D. Hooper and T. Plehn, Phys. Lett. **B562** (2003) 18 and G. Belanger, F. Boudjema, A. Pukhov and S. Rosier-Lees, arXiv:hep-ph/0212227.
- [16] H. Bachacou, I. Hinchliffe and F. E. Paige, Phys. Rev. D **62**, 015009 (2000).
- [17] B. C. Allanach, C. G. Lester, M. A. Parker and B. R. Webber, JHEP **0009**, 004 (2000).
- [18] B. K. Gjelsten, D. J. Miller and P. Osland, JHEP **0412** (2004) 003.

- [19] M. M. Nojiri, G. Polesello and D. R. Tovey, JHEP **0603**, 063 (2006).
- [20] A. Datta, A. Djouadi, M. Guchait and Y. Mambrini, Phys. Rev. D **65**, 015007 (2002); K. Huitu, J. Laamanen, P. N. Pandita and S. Roy, Phys. Rev. D **72**, 055013 (2005).
- [21] F. E. Paige, S. D. Protopopescu, H. Baer and X. Tata, arXiv:hep-ph/0312045.
- [22] W. Beenakker, R. Hopker and M. Spira, arXiv:hep-ph/9611232;
W. Beenakker, R. Hopker, M. Spira and P. M. Zerwas, Nucl. Phys. B **492** (1997) 51.
- [23] A. Bottino, N. Fornengo, G. Polesello and S. Scopel (to appear).